Science of the Total Environment 842 (2022) 156852

Contents lists available at ScienceDirect

Science of the Total Environment

journal homepage: www.elsevier.com/locate/scitotenv

ALOS-2 L-band SAR backscatter data improves the estimation and temporal transferability of wildfire effects on soil properties under different post-fire vegetation responses

José Manuel Fernández-Guisuraga [a,*], Elena Marcos [a], Susana Suárez-Seoane [b], Leonor Calvo [a]

[a] Area of Ecology, Department of Biodiversity and Environmental Management, Faculty of Biological and Environmental Sciences, University of León, 24071 León, Spain
[b] Department of Organisms and Systems Biology, Ecology Unit, Research Institute of Biodiversity (IMIB; UO-CSIC-PA), University of Oviedo, Oviedo, Mieres, Spain

HIGHLIGHTS

- SAR data were novelty used for mapping soil organic C, N and P in burned landscapes.
- L-band SAR data outperformed C-band SAR data to retrieve soil properties after fire.
- ALOS-2 predictive relationships were transferable between post-fire scenarios.
- The changes in soil properties after fire depended on the plant community type.

GRAPHICAL ABSTRACT

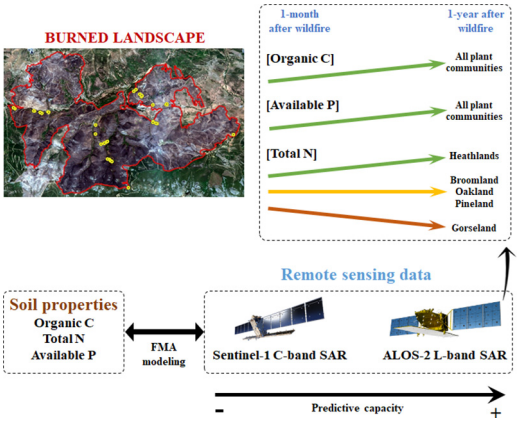

ARTICLE INFO

Editor: Manuel Esteban Lucas-Borja

Keywords:
Digital soil mapping
Nitrogen
Phosphorous
Organic carbon
Synthetic aperture radar
Wildfire

ABSTRACT

Remote sensing techniques are of particular interest for monitoring wildfire effects on soil properties, which may be highly context-dependent in large and heterogeneous burned landscapes. Despite the physical sense of synthetic aperture radar (SAR) backscatter data for characterizing soil spatial variability in burned areas, this approach remains completely unexplored. This study aimed to evaluate the performance of SAR backscatter data in C-band (Sentinel-1) and L-band (ALOS-2) for monitoring fire effects on soil organic carbon and nutrients (total nitrogen and available phosphorous) at short term in a heterogeneous Mediterranean landscape mosaic made of shrublands and forests that was affected by a large wildfire. The ability of SAR backscatter coefficients and several band transformations of both sensors for retrieving soil properties measured in the field in immediate post-fire situation (one month after fire) was tested through a model averaging approach. The temporal transferability of SAR-based models from one month to one year after wildfire was also evaluated, which allowed to assess short-term changes in soil properties at large scale as a function of pre-fire plant community type. The retrieval of soil properties in immediate post-fire conditions featured a higher overall fit and predictive capacity from ALOS-2 L-band SAR backscatter data than from Sentinel-1 C-band SAR data, with the absence of noticeable under and overestimation effects. The transferability of the ALOS-2 based model to one year after wildfire exhibited similar performance to that of the model calibration scenario (immediate post-fire conditions). Soil organic carbon and available phosphorous content was significantly higher one year after wildfire than immediately after the fire disturbance. Conversely, the short-term change in soil total

* Corresponding author.
E-mail address: jofeg@unileon.es (J.M. Fernández-Guisuraga).

http://dx.doi.org/10.1016/j.scitotenv.2022.156852
Received 28 April 2022; Received in revised form 15 June 2022; Accepted 16 June 2022
Available online 22 June 2022

nitrogen was ecosystem-dependent. Our results support the applicability of L-band SAR backscatter data for monitoring short-term variability of fire effects on soil properties, reducing data gathering costs within large and heterogeneous burned landscapes.

1. Introduction

Soils are the main reservoir of macronutrients in terrestrial ecosystems, such as nitrogen (N) and phosphorus (P), and of organic carbon (C), delivering multiple functions and ecosystem services (Maestre et al., 2012). For instance, soil organic C plays an essential role in global C cycling of the earth system since it constitutes an important atmospheric sink (Stockmann et al., 2013; Liang et al., 2019) with strong implications in climate change mitigation (Luo et al., 2017). In agroforestry systems, soil organic C is also closely linked to soil quality and fertility (Wang et al., 2020). On their hand, soil N and P are the most important macronutrients limiting terrestrial ecosystems' productivity (Rossel and Bui, 2016). Specifically, both nutrients have a strong impact on the dynamics of soil C stocks and C cycling in forest ecosystems worldwide (Holdo et al., 2012; Yang et al., 2019) through controls on net primary productivity (Fernandez-Martinez et al., 2014), decomposition rates (Wang et al., 2010) and soil microbial activity (Liu et al., 2010).

Wildfires are recurrent disturbances in the Mediterranean Basin (Pausas and Keely, 2009), entailing shifts in the multifunctionality of terrestrial ecosystems (Lucas-Borja et al., 2021) related to ecological impacts on vegetation communities composition and structural characteristics (Fernández-Guisuraga et al., 2019a), soil properties (Alcañiz et al., 2018; Fernández-García et al., 2019) and ecosystem nutrient cycling (Johnson and Turner, 2019). In forest ecosystems of the Mediterranean Basin, fire-induced changes in organic and mineral soil layers have proven to be highly context-dependent as a function of plant community type (Fernández-García et al., 2019; Huerta et al., 2020), soil characteristics (Knicker, 2007), microscale variation of soil burn severity (Johnstone and Chapin, 2006) and environmental conditions (Vieira et al., 2015). Therefore, the identification of fire effects on soil properties through field sampling campaigns is not functional for assessing large burned landscapes (Hudak et al., 2007) due to the fine scale of variation of soil effects (Morgan et al., 2014), even more when dealing with high environmental variability regarding pre-fire plant communities (Yang et al., 2019).

Remote sensing techniques (RST) based on multispectral and hyperspectral passive optical data acquired from space-borne and aerial platforms have been extensively used for obtaining spatially-explicit maps of soil properties in agroforestry systems. For instance, recent studies (e.g. Minu et al., 2017; Kovács et al., 2021; Mzid et al., 2022) used data acquired from Earth Observing-1 (EO-1) and PRISMA hyperspectral satellite missions for predicting and mapping successfully soil organic C, total N and available P content in croplands and forests worldwide. Remote sensing data acquired from multispectral sensors on-board Sentinel-2 and Landsat-7 satellite missions, as well as from multispectral cameras on-board unmanned aerial vehicles (UAVs), have also been used for digital soil mapping (e.g. Aldana-Jague et al., 2016; Mirzaee et al., 2016; Gholizadeh et al., 2018; Zhou et al., 2021). However, the remote estimation of soil properties using multispectral and hyperspectral passive sensors might be restricted to indirect correlations in vegetated areas, since the reflectance signal is mostly determined by top-of-canopy traits (Fernández-Guisuraga et al., 2021b). In this sense, the close relationship between vegetation biophysical characteristics and soil properties (Zhou et al., 2020) drives the prediction of soil spatial variability through optical remotely sensed vegetation features (Yang et al., 2019), with this behavior leading to soil properties overestimation (Angelopoulou et al., 2019). To deal with this constraint, active remote sensing backscatter acquired by microwave synthetic aperture radar (SAR) instruments are among the most reliable RST for digital mapping of soil properties (Wang et al., 2020; Schönbrodt-Stitt et al., 2021). First, SAR data acquisitions are relatively independent of weather and solar illumination (Liu et al., 2013). Second, improved sensor characteristics offer nowadays dual polarization SAR data and increased spatial resolution (Belenguer-Plomer et al., 2019). Third, SAR signal can penetrate the soil through vegetation canopy, especially with increasing wavelength (Jagdhuber, 2012) and, depending on canopy closure and architecture, as well as incident angles (Inoue et al., 2002). For these reasons, the recently launched satellite missions Sentinel-1 C-band (5.6 cm) SAR of the European Space Agency (ESA) and ALOS-2 L-band (23.6 cm) SAR of the Japan Aerospace Exploration Agency (JAXA), are been increasingly used to characterize the spatial variability of soil properties in crop fields and woodlands (e.g. Bartsch et al., 2016; El Hajj et al., 2019; Yang et al., 2019; Yang and Guo, 2019; Schönbrodt-Stitt et al., 2021), sometimes fused with passive optical data (e.g. Ceddia et al., 2017; Bousbih et al., 2019; Wang et al., 2020).

In the field of remote sensing monitoring of fire disturbances, SAR backscatter data have been used to map wildfire scars (e.g. Belenguer-Plomer et al., 2019; Tanase et al., 2020) and fire severity (e.g. Tanase et al., 2014, 2015; Philipp and Levick, 2020) with high reliability. Recently, the European Union soil strategy recommended stepping up efforts in mapping and assessing soil organic C and nutrients content past disturbances (European Commission, 2021). Nonetheless, the characterization of soil spatial variability in burned areas through RST, and particularly leveraging SAR strengths for this purpose, remains completely unexplored. In this sense, the potential of SAR backscatter data in different bands (i.e. wavelengths) for mapping immediate post-fire effects on soil properties should be addressed. The transferability of the predictive relationships between soil properties and SAR data across different time periods after wildfire and, hence, with different vegetation responses (Hudak et al., 2007), should also be investigated since the development of transferable RST has been one of the most demanded resources by land managers in recent years (Fernández-Guisuraga et al., 2019b).

In this paper, we aimed to evaluate the potential of SAR backscatter data in different bands to assess the effects of a large wildfire on soil properties in a landscape mosaic located at the western Mediterranean Basin that was made of several shrubland and forest plant communities. Specifically, we aimed to: (i) compare the efficiency of C-band and L-band SAR data to quantitatively estimate soil organic C, total N and available P immediately after fire under high pre-fire plant community heterogeneity; (ii) evaluate the temporal transferability of the identified predictive relationships between soil properties and SAR data; and, (iii) assess the effects of pre-fire plant community type on the short-term changes of post-fire soil properties.

2. Material and methods

2.1. Study site

The study site is located within a wildfire perimeter that burned 9940 ha of shrubland and forest communities in the Sierra de Cabrera mountain range (north-northwestern Iberian Peninsula; Fig. 1) between 21th and 27th August 2017. The relief of the study site is rough and complex, with prominent crests and valleys with steep slopes, ranging at an elevation between 836 and 1938 m above sea level. Soils are acidic and classified as Lithic (LPq) and Distric (LPd) Leptosols, and Distric (CMd) and Humic (CMu) Cambisols (GEODE, 2022; ITACyL, 2022). Climate is Mediterranean temperate, with mean temperature and precipitation values ranging between 600–1500 mm and 5–15 °C for a 50-year period, respectively (Ninyerola et al., 2005). Several plant communities were affected by the wildfire: (i) *Genista hystrix* Lange (gorse) shrublands; (ii) *Erica australis* L. heathlands; (iii) *Genista florida* L. (broom) shrublands; (iv) *Quercus pyrenaica* Willd. (Pyrenean oak) forests; and (v) *Pinus sylvestris* L. (Scots pine) forests.

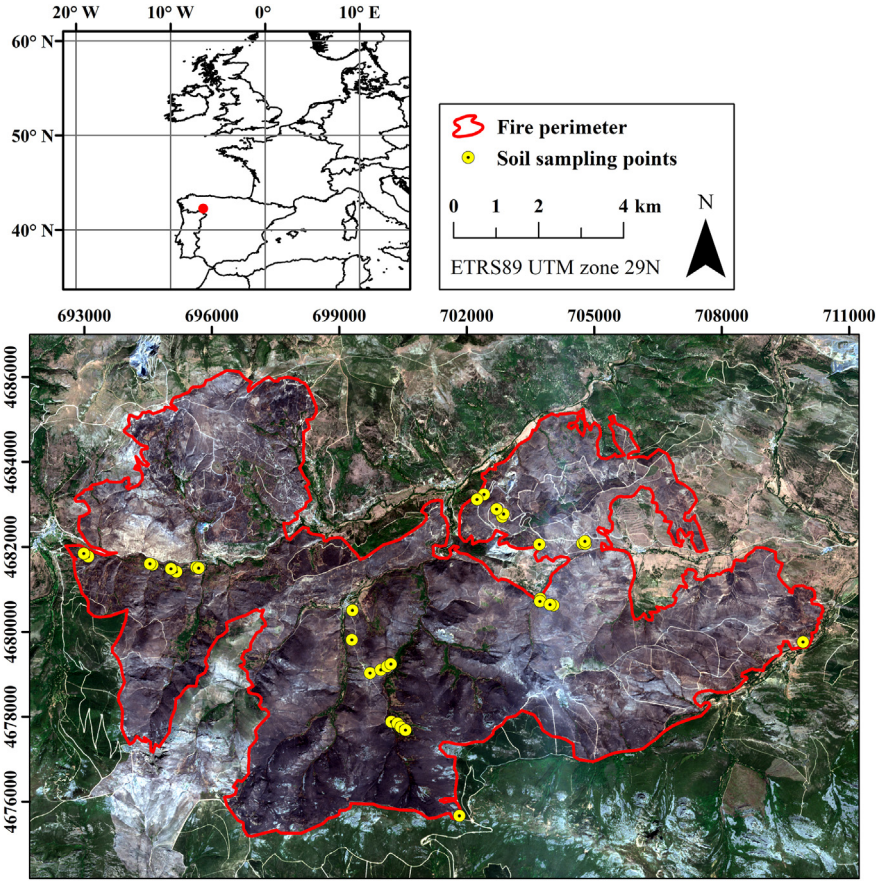

Fig. 1. Wildfire of Sierra de Cabrera (NW Spain) and location of the soil sampling points.

2.2. Soil sampling and analyses

A set of 35 field plots of 30 m × 30 m with a minimum separation of 200 m was established in gorse, heathland and Pyrenean oak plant communities following a random design using the plant communities as strata (Table 1). Plots were located in homogeneous areas regarding vegetation legacies and soil characteristics, and were geolocated with a sub-meter accuracy GPS receiver ($RMSE_{X,Y}$ < 0.50 m). Specifically, we surveyed the 35 plots and acquired soil samples the month following the wildfire (September 2017), and 19 plots one year after wildfire (July 2018) for validation purposes.

Two composite soil samples (integrated by four subsamples) were systematically collected within each plot for obtaining a representative sample, i.e. one at NW and the other at SE, separated by 20 m. Soil samples were collected using a soil sampler tool with a diameter of 7 cm and a depth of 3 cm, since fire effects on soil properties are mostly limited to the uppermost 3 cm (Moreno and Oechel, 1994). Vegetation legacies, litter and charred debris were removed before collecting samples. Soil samples were air dried and mesh-sieved (2 mm) in the laboratory, and stored for 2–3 months at 20 °C until analyses.

Soil organic C (%) was determined using an EuroVector EA3000 elemental analyzer (EuroVector SpA, Italy) following the combustion approach (Dumas, 1831). We analyzed soil total N (%) using the Kjeldahl method (Bremner and Mulvaney, 1982) and a DK 20 digestion unit (VELP Scientifica Srl, Italy). Finally, we determined available P (AP; mg/kg) through the Olsen et al. (1954) procedure at 882 nm using a UV Mini 1240 spectrophotometer (Shimadzu Corporation, Japan). Soil organic C and nutrients content for each plant community are shown in Table 1.

Table 1
Descriptive statistics of the soil properties surveyed in the field one month and one year after fire.

Plant community	One month after fire					One year after fire				
	# of plots	Mean	Min	Max	SD	# of plots	Mean	Min	Max	SD
Gorse	8 plots					5 plots				
Organic C (%)		5.76	3.03	9.91	2.07		4.48	3.45	6.26	1.11
Total N (%)		0.46	0.27	0.72	0.13		0.37	0.31	0.48	0.08
Available P (mg/kg)		24.3	9.95	57.05	14.5		17.38	7.31	33.06	9.37
Heathland	11 plots					6 plots				
Organic C (%)		7.94	1.58	25.31	7.09		7.46	5.37	9.12	1.91
Total N (%)		0.46	0.11	1.17	0.31		0.45	0.36	0.52	0.08
Available P (mg/kg)		28.61	14.03	68.66	15.85		23.34	12.51	39.53	14.29
Pyrenean oak	16 plots					8 plots				
Organic C (%)		11.64	4.27	33.97	6.89		7.48	5.94	9.91	1.33
Total N (%)		0.73	0.38	1.64	0.3		0.52	0.37	0.67	0.09
Available P (mg/kg)		62.82	19.61	128.78	39.24		29.71	15.47	57.78	13.27

2.3. SAR data and processing

Remote sensing SAR data used to predict soil properties one month and one year after wildfire included Sentinel-1 C-band and ALOS-2 L-band backscatter at dual polarization, as well as several arithmetical combinations of both polarizations for each sensor. Since SAR backscatter behavior both in C-band and L-band is heavily influenced by soil moisture (Williams et al., 2022), particularly in the early post-fire period (Tanase et al., 2015; Belenguer-Plomer et al., 2019), the cumulative precipitation for a seven-day period prior to SAR image acquisition was collected from the meteorological stations closest to the study area (two stations within 40 km radius) (AEMET, 2022). No precipitation was registered during the imagery acquisition period. Therefore, a low spatial variability of soil moisture in the uppermost centimeters was expected (Tanase et al., 2015).

2.3.1. Sentinel-1 data

Sentinel-1 is the Copernicus SAR missions of the ESA. It comprises a constellation of two C-band (5.6 cm) SAR polar-orbiting satellites: Sentinel-1A and Sentinel-1B, launched on April 2014 and April 2016, respectively. Sentinel-1 satellite constellation operates in four acquisition modes with different resolution and coverage, being interferometric wide swath and wave the default modes over land and open ocean, respectively. Additionally, the C-band SAR instrument supports operation in single and dual polarization (ESA, 2022a). The Sentinel-1A SAR scenes covering the study site were downloaded from the Copernicus Open Access Hub on 6th October 2017 (around one month after fire) and 21th July 2018 (approximately one year after fire) (ascending orbit; relative orbit number: 74) in interferometric wide swath mode at dual polarization (VV + VH). The SAR images corresponded to a Ground Range Detected (GRD) Level-1 product (ESA, 2022b). This product was pre-processed using the Sentinel-1 Toolbox (S1TBX) integrated within Sentinel Application Platform (SNAP; ESA, 2022c). First, digital number values were converted to radiometrically calibrated backscatter (radar brightness or beta nought; β^0) using the information provided in the product metadata. Second, β^0 VV and VH backscatter bands were multi-looked to the nominal Sentinel-1 resolution (20 m square pixels). Third, a terrain-flattening correction was applied to remove the radiometric variability associated with topography (Small, 2011), obtaining gamma nought (γ^0) backscatter coefficients of VV and VH polarizations. Fourth, the calibrated images were orthorectified to ground geometry by means of the range Doppler method (Small and Schubert, 2008). Finally, γ^0 backscatter intensity values in linear scale were converted to dB units using a logarithmic transformation. In addition to VV and VH γ^0 backscatter coefficients, we computed several band transformations as potential predictors of soil properties (Yang and Guo, 2019; Yang et al., 2019; Nguyen et al., 2022): VV / VH, VH / VV, VV − VH, VV + VH, VV × VH, (VV + VH) / 2, and the radar forest degradation index (RFDI; Mitchard et al., 2012). Sentinel-1 predictors were extracted for each 30 m × 30 m field plot by averaging the values of a regular grid of points systematically sampled within each plot, totaling 36 points with a spacing of 5 m and 2.5 m apart from the plot edge (Picotte and Robertson, 2011).

2.3.2. ALOS-2 data

ALOS-2 mission was launched on May 2014 by JAXA, being a follow-on L-band SAR satellite mission of ALOS-1, which suffered a power failure in April 2011 (Zhang et al., 2019). ALOS-2 operates at a wavelength of 23.6 cm and has three acquisition modes (spotlight, stripmap and scanSAR) with varying spatial resolutions and single, dual and quad polarization (JAXA, 2022). Starting from 2015, JAXA has delivered 25 m ALOS-2 PALSAR-2 annual global mosaics of Fine Beam Dual-polarization (FBD) SAR data strips (stripmap mode) acquired in ascending orbits with HH and HV polarizations (Bouvet et al., 2018; Santoro et al., 2022). Mosaic data for the study site were acquired on 3rd October 2017 and 24th July 2018 (i.e., around one month and one year after fire, respectively) from JAXA Earth Observation Research Center (https://www.eorc.jaxa.jp/). The product was pre-processed by JAXA within the mosaicking algorithm developed by Shimada and Ohtaki (2010), which includes radiometric calibration, terrain-flattening correction and orthorectification. ALOS-2 image was co-registered with respect to Sentinel-1 image in SNAP using a cross correlation operator and a third-degree polynomial warp function (Tanase et al., 2015). Product data stored in digital numbers were converted to γ^0 backscatter intensity in dB units (Eq. (1)).

$$\gamma^0(dB) = 10\ log\ _{10}\left(DN^2\right) + CF \quad (1)$$

where DN are the digital numbers and CF is a calibration factor equal to −83 dB for PALSAR-2. Analogous to Sentinel-1, several band transformations were calculated besides the HH and HV γ^0 backscatter coefficients: HH / HV, HV / HH, HH − HV, HH + HV, HH × HV, (HH + HV) / 2, and the RFDI. The values of ALOS-2 predictors were extracted for each 30 m × 30 m field plot following the same procedure as for Sentinel-1.

2.4. Data analysis

The content of soil organic C, total N and available P one month after fire was modeled on the basis of Sentinel-1 and ALOS-2 predictors using a frequentist model averaging approach (FMA; Burnham and Anderson, 2002). This technique features weighted parameter estimates from the candidate models in the full model set rather than relying on estimates from a single model (Nakagawa and Freckleton, 2011). The approach allows to account for the uncertainty linked to the model selection process unlike traditional variable selection approaches (Whittingham et al., 2006). In this sense, FMA provides a robust and reliable handling of uncertainty in model parametrization and structure (Burnham and Anderson, 2002; Nakagawa and Freckleton, 2011) which, in turn, contributes to an improved predictive capacity through reduced variance and bias than the individual candidate models (Dormann et al., 2018).

Although FMA approaches are less sensitive than single models to multicollinearity issues (Freckleton, 2010), we followed a conservative approach and identified strongly correlated groups of predictors within Sentinel-1 and ALOS-2 backscatter coefficients and band transformations through bivariate Pearson correlations ($r_{Pearson} > |0.7|$) (Fig. SM1). Within each group of correlated band transformations, we preserved those that explained the greatest variance in univariate Generalized Linear Models (GLMs) (Table SM1). As a result of this analysis, we retained: (i) VV and VH backscatter coefficients and VH/VV ratio as Sentinel-1 predictors, and (ii) HH and HV backscatter coefficients and HV/HH ratio for ALOS-2.

For each soil property (soil organic C, total N and available P), candidate models were fitted separately for each sensor using multivariate GLMs following a Gamma error distribution with a log-link function (Zuur et al., 2009). We included linear and quadratic terms in GLMs to consider potential non-linear relationships. Therefore, the entire model space (i.e. the number of candidate models) for each soil property and SAR sensor was fully enumerated by iterating all possible predictor combinations, including polynomials (2^6 distinct subsets). Since it is not advisable to average the full model set because of (i) spurious parameter estimates from models with low weights (Grueber et al., 2011) and (ii) excessive model uncertainty with a large model set and low sample size (Burnham and Anderson, 2002), we defined a top model set to average. Following the proposal of Burnham and Anderson (2002), we retained the models with a Δ-value <2 of the Akaike Information Criterion adapted for small sample sizes (AIC_c; Hurvich and Tsai, 1989). The estimate and standard error of a parameter were set to zero in those models of the top model set where it is absent in order to decrease the size effect of predictors that only appear in models with low weights (Grueber et al., 2011).

FMA performance was evaluated by means of the R-squared (R^2), the root-mean-squared error (RMSE) and the normalized RMSE (nRMSE), from the maximum and minimum observation value, for the relationship between observed and predicted values (internal model validation). The relationship between soil properties and predictors was visualized through scatterplots for disentangling the behavior of SAR backscatter across different bands and polarizations. The best performing model (either Sentinel-1

or ALOS-2) was used to produce a spatially-explicit map of soil organic C, total N and available P of the study site in immediate post-fire situation. The best models for each soil property, calibrated one month after fire, were extrapolated to predict spatial variability of soil properties one year after wildfire (external model validation). Model transferability performance was evaluated through the R^2, RMSE and nRMSE.

A plant community classification map developed by Fernández-Guisuraga et al. (2021a) for the study site, along with the maps of soil properties developed in this study, were used to evaluate short-term changes in soil properties (one month to one year after fire) as a function of plant community type. The plant community map was computed from a pre-fire Sentinel-2 scene classified using the maximum likelihood (ML) algorithm (Strahler, 1980). The overall accuracy of the classification was equal to 91 %. See Fernández-Guisuraga et al. (2021a) for more details of the procedure.

A random sampling of 10,000 points stratified by plant community type was conducted within the fire perimeter to extract soil organic C, total N and available *P* values one month and one year after wildfire. We ensured a minimum distance of 30 m between points. We implemented a two-way repeated measures ANOVA for assessing the effect of plant community type on the short-term changes of post-fire soil properties. Subsequently, a Tukey's HSD test was performed for determining the significance of the differences in soil properties both: (i) between plant communities in each time period, and (ii) within each community between the two time periods.

All statistical analyses were implemented in R (R Core Team, 2021) using the "MuMIn" (Barton, 2020), "caret" (Kuhn, 2020), "raster" (Hijmans, 2021), "rgdal" (Bivand et al., 2021) and "rstatix" (Kassambara, 2021) packages.

3. Results

3.1. Prediction of soil properties one month after fire from C-band and L-band SAR data

ALOS-2 L-band SAR backscatter data featured a higher overall fit (R^2 = 0.42–0.60) and predictive capacity (nRMSE = 12.5–21.7 %) than Sentinel-1 C-band SAR (R^2 = 0.17–0.20 and nRMSE = 17.3–25.3 %) for predicting soil properties one month after fire (Table 2). The soil property predicted at best by ALOS-2 SAR data was soil organic C (nRMSE = 12.5 %), followed by total N (nRMSE = 13.7 %) and available P (nRMSE = 21.7 %).

All the considered ALOS-2 predictors (HH and HV backscatter, and HV/HH ratio) were selected as important variables in the soil organic C, total N and available P models (Table 3), usually with high significance (*p*-values ≤ 0.01). Conversely, Sentinel-1 predictors (VV and VH backscatter, and VH/VV ratio) were all included only in the soil organic C model. For the case of the total N and available P models, only Sentinel-1 VH backscatter was selected as a relevant predictor (Table 3). The relationships between Sentinel-1 and ALOS-2 backscatter and soil properties were mostly quadratic and direct (Table 3 and Fig. 2), being noticeable the strength of the correlation of the ALOS-2 HH polarization with all soil properties (R^2 > 0.3) (Fig. 2).

Soil organic C, total N and available P model predictions one month after fire based on ALOS-2 fitted data (internal model validation) were more closely tailored to the 1:1 line than models calibrated with Sentinel-1 (Fig. 3). In this sense, a substantial underestimation at high observed values for all soil properties was evidenced from Sentinel-1 based models, this effect being much less noticeable in ALOS-2 models (Fig. 3).

Spatially explicit prediction maps of soil properties one month after fire were computed from FMA predictions applied to ALOS-2 backscatter data (Fig. 4A). The mean soil organic C, total N and available *P* values within the burned scar one month after fire were 4.78 %, 0.65 % and 34.13 mg/kg, respectively.

Table 2
Frequentist model averaging (FMA) performance of soil organic C, total N and available P evaluated through the R-squared (R^2), root-mean-squared error (RMSE) and normalized RMSE (nRMSE) one month after fire.

	Soil organic C		Soil total N		Available P	
	Sentinel-1	ALOS-2	Sentinel-1	ALOS-2	Sentinel-1	ALOS-2
R^2	0.173	0.597	0.201	0.496	0.202	0.415
RMSE	5.825	4.061	0.265	0.210	30.103	25.778
nRMSE	18.6 %	12.5 %	17.3 %	13.7 %	25.3 %	21.7 %

Table 3
Average model outputs computed from the frequentist model averaging (FMA) approach for soil organic C, total N and available P one month after fire using as predictors both Sentinel-1 and ALOS-2 backscatter data.

Response variable	Parameter	Estimate	Standard error	z value	p-Value
Soil organic C	(Intercept)	28.391	24.576	1.133	0.257
	Sentinel-1 VH	2.737	3.814	0.701	0.483
	(Sentinel-1 VH)^2	0.044	0.120	0.358	0.721
	Sentinel-1 VV	1.272	0.608	2.021	**0.043**
	(Sentinel-1 VV)^2	−0.050	0.024	2.015	**0.044**
	Sentinel-1 VH/VV	−5.333	4.175	1.226	0.220
	(Intercept)	−19.746	24.504	0.796	0.426
	ALOS-2 HV	2.383	1.205	1.944	**0.052**
	(ALOS-2 HV)^2	0.035	0.029	1.161	0.246
	ALOS-2 HH	−4.096	1.565	2.511	**0.012**
	(ALOS-2 HH)^2	0.076	0.027	2.706	**0.007**
	ALOS-2 HV/HH	33.455	10.478	3.112	**0.002**
	(ALOS-2 HV/HH)^2	7.046	1.418	4.763	**0.000**
Soil total N	(Intercept)	2.290	1.896	1.188	0.235
	Sentinel-1 VH	0.205	0.226	0.890	0.374
	(Sentinel-1 VH)^2	0.005	0.007	0.667	0.505
	(Intercept)	0.878	1.270	0.687	0.492
	ALOS-2 HV	0.094	0.041	2.257	**0.024**
	ALOS-2 HH	0.129	0.167	0.767	0.443
	(ALOS-2 HH)^2	0.005	0.002	2.062	**0.039**
	ALOS-2 HV/HH	0.957	0.598	1.579	0.114
	(ALOS-2 HV/HH)^2	0.179	0.121	1.453	0.146
Available P	(Intercept)	119.293	38.035	3.065	**0.002**
	Sentinel-1 VH	5.602	1.985	2.711	**0.007**
	(Sentinel-1 VH)^2	−0.153	0.055	2.669	**0.008**
	(Intercept)	522.233	288.418	1.770	0.077
	ALOS-2 HV	5.608	5.328	1.038	0.299
	(ALOS-2 HV)^2	−0.067	0.024	2.649	**0.008**
	ALOS-2 HH	−2.301	10.215	0.223	0.824
	(ALOS-2 HH)^2	−0.154	0.057	2.575	**0.010**
	ALOS-2 HV/HH	−616.603	263.193	2.250	**0.024**
	(ALOS-2 HV/HH)^2	165.784	84.627	1.904	0.057

Bold p-values denote statistical significance at the 0.05 level.

3.2. Temporal transferability of L-band SAR predictive relationships from one month to one year after fire

External model validation based on the transferability of predictive relationships estimated with ALOS-2 backscatter data (highest-performing model in internal validation) to one year after wildfire provided encouraging results. The RMSE was similar or even lower for soil organic C (1.4 %), total N (0.1 %) and available P (24.0 mg/kg) (Fig. 5) than in the immediate post-fire situation (Table 2), with no apparent over or underestimation effects for the entire range of field-measured soil properties. The mean change in soil organic C, total N and available P content between one month and one year after fire, computed from ALOS-2 backscatter predictions (Fig. 4B), was 8.82 %, 0.06 % and 38.53 mg/kg, respectively.

3.3. Effect of pre-fire plant community type on the short-term changes of soil properties

The magnitude of change in soil properties from one month to one year after wildfire depended on the plant community type (Fig. 6), as resulted from the significant interactions (*p*-values < 0.05) between community

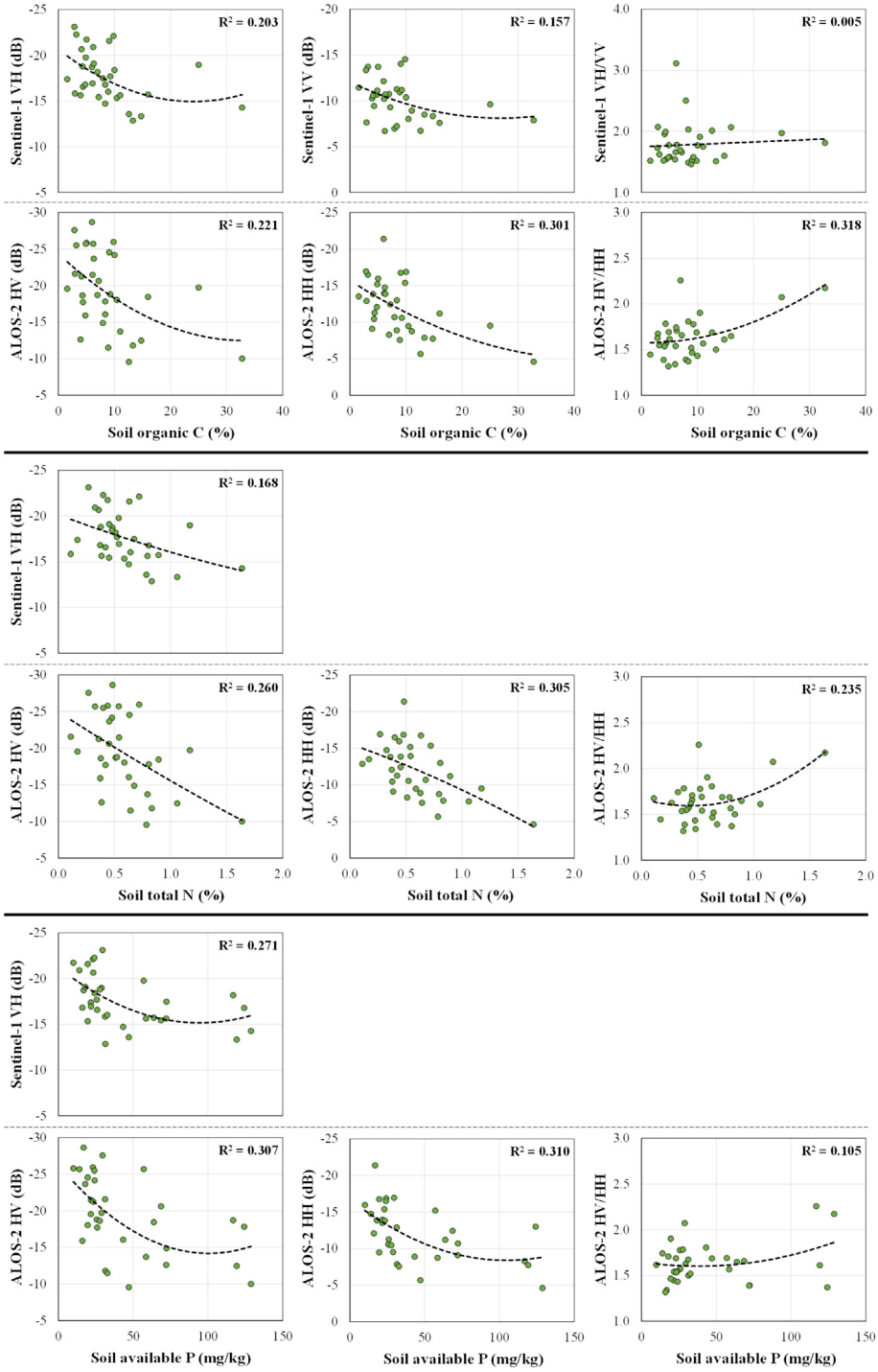

Fig. 2. Relationship between Sentinel-1 and ALOS-2 backscatter predictors included in average models of frequentist model averaging (FMA) approach (Table 3) and soil organic C, total N and available P one month after fire.

type and time in the two-way repeated measures ANOVA for each analyzed soil property. Soil organic C and available *P* values were significantly higher (p-values < 0.001) one year after wildfire in all plant communities. In contrast, soil total N increased significantly in heathlands (p-value < 0.001), but decreased in gorse shrublands (p-value < 0.05). No significant differences were detected in the remaining plant communities. One month after fire, the highest values registered for soil properties corresponded to Pyrenean oak forests, while one year after wildfire, heathlands and Scots pine forests exhibited similar values to Pyrenean oak forests for all soil properties.

4. Discussion

4.1. Prediction of soil properties by C-band and L-band SAR data

The operating wavelength of SAR instruments had a large impact on the prediction performance of soil properties immediately after wildfire. Overall, the retrieval of soil organic C and nutrients content from ALOS-2 L-band SAR backscatter data clearly outperformed the retrieval from Sentinel-1 C-band SAR data. At shorter wavelengths (i.e. Sentinel-1 C-band at 5.6 cm), the backscatter signal is dominated by volume and direct scattering from

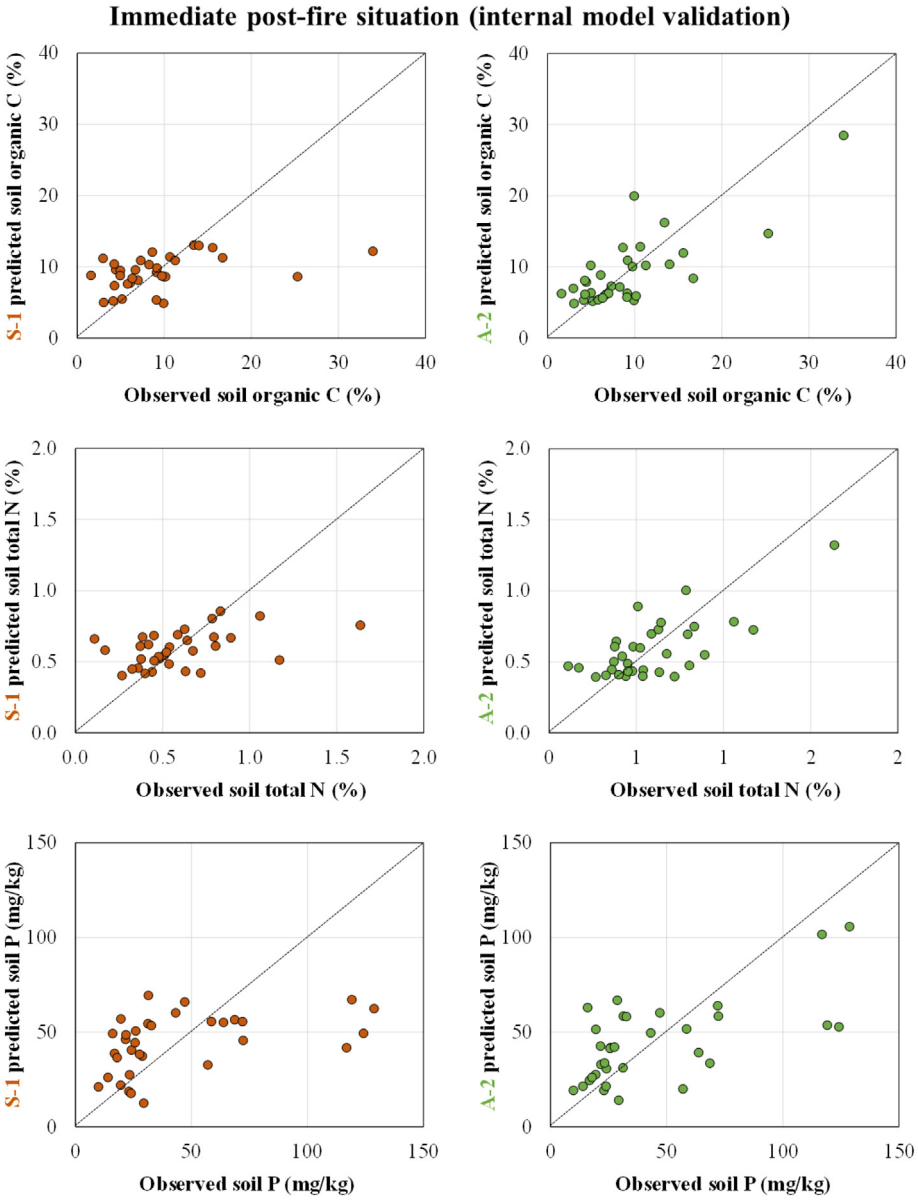

Fig. 3. Relationship between observed and predicted soil organic C, total N and available P one month after fire from Sentinel-1 (S-1) and ALOS-2 (A-2) backscatter data using a frequentist model averaging approach. Overall fit and predictive statistics are displayed in the Table 2.

the uppermost part of the vegetation canopy (Tanase et al., 2010). In contrast, with L-band SAR instruments, operating at longer wavelengths (i.e. 23.6 cm of the SAR instrument on-board ALOS-2), an increased interaction with soil surface properties can be expected (Tanase et al., 2014), namely soil moisture and surface roughness (Pulliainen et al., 1996; Zribi and Dechambre, 2003), these properties being themselves highly correlated with soil C and nutrients content (e.g. Moser et al., 2009). In addition, the strength of the correlation of the individual ALOS-2 HH polarization with all soil properties could be explained by the higher sensitivity of co-polarized L-band SAR backscatter to soil dielectric properties as compared to cross-polarized backscatter (Burgin et al., 2011; Mermoz et al., 2015; Tanase et al., 2015).

Despite the characterization of soil spatial variability in burned areas using SAR backscatter remained unexplored to date, several studies used Sentinel-1, ALOS-1 or ALOS-2 data for mapping soil properties in croplands and wildland areas worldwide (Zhou et al., 2020; Le et al., 2021; Nguyen et al., 2022). The retrieval performance in these works was consistent with that of the present study using Sentinel-1 C-band backscatter data (R^2 = 0.17–0.20). For their part, Ceddia et al. (2017) and Wang et al. (2020) mapped the spatial distribution of soil organic C using ALOS-1 backscatter data in wildland areas of the central region of the Amazonas and in Spain, respectively. The higher retrieval performance observed in this study for capturing the spatial variability in soil properties using ALOS-2 L-band backscatter data (R^2 = 0.42–0.60 vs. R^2 = 0.11–0.20) could be explained by the partial or total consumption of canopy foliage and small branches in burned landscapes, being L-band radar measurements even more sensitive to the backscatter properties of the underlying ground (Tanase et al., 2010). Several of the abovementioned studies have also developed additional modeling strategies based on SAR and multispectral remote sensing data fusion, improving the retrieval performance of soil properties in most cases. Nevertheless, the differential vegetation legacies responses in burned landscapes would lead to inconsistencies on the indirect vegetation-soil relationships modeled from passive remote sensing data (Maynard and Levi, 2017) and, therefore, a data fusion modeling approach was not addressed in this study. Future research should consider the impact of local incidence angle and soil surface roughness on the estimation of soil properties in burned landscapes, since these variables are known to greatly influence the SAR signal sensitivity to fire effects (Bourgeau-Chavez et al., 2007;

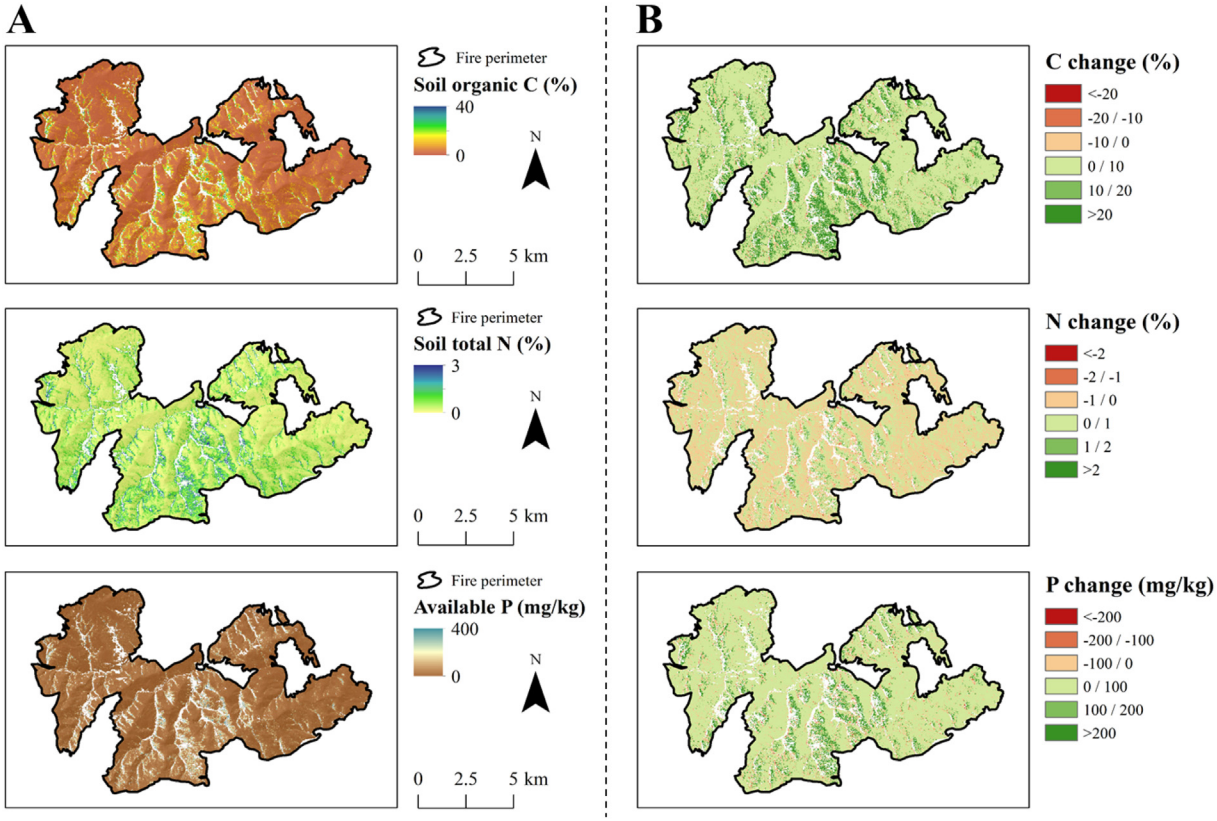

Fig. 4. Spatially explicit maps (spatial resolution of 25 m) of predicted soil organic C, total N and available P by the frequentist model averaging (FMA) approach using ALOS-2 predictors one month after fire (A). The magnitude of change in soil properties between one month and one year after fire is also displayed (B). Blank regions within the fire perimeter correspond to unburned valley-bottom areas.

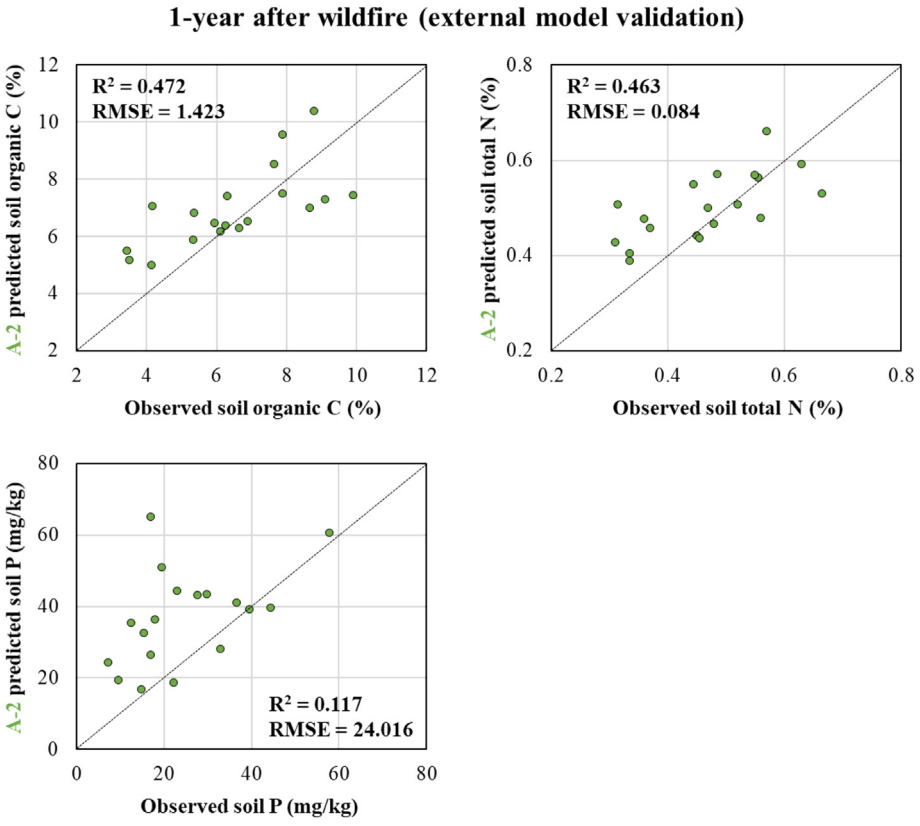

Fig. 5. Relationship between observed and predicted soil organic C, total N and available P one year after fire from ALOS-2 backscatter data using a frequentist model averaging approach.

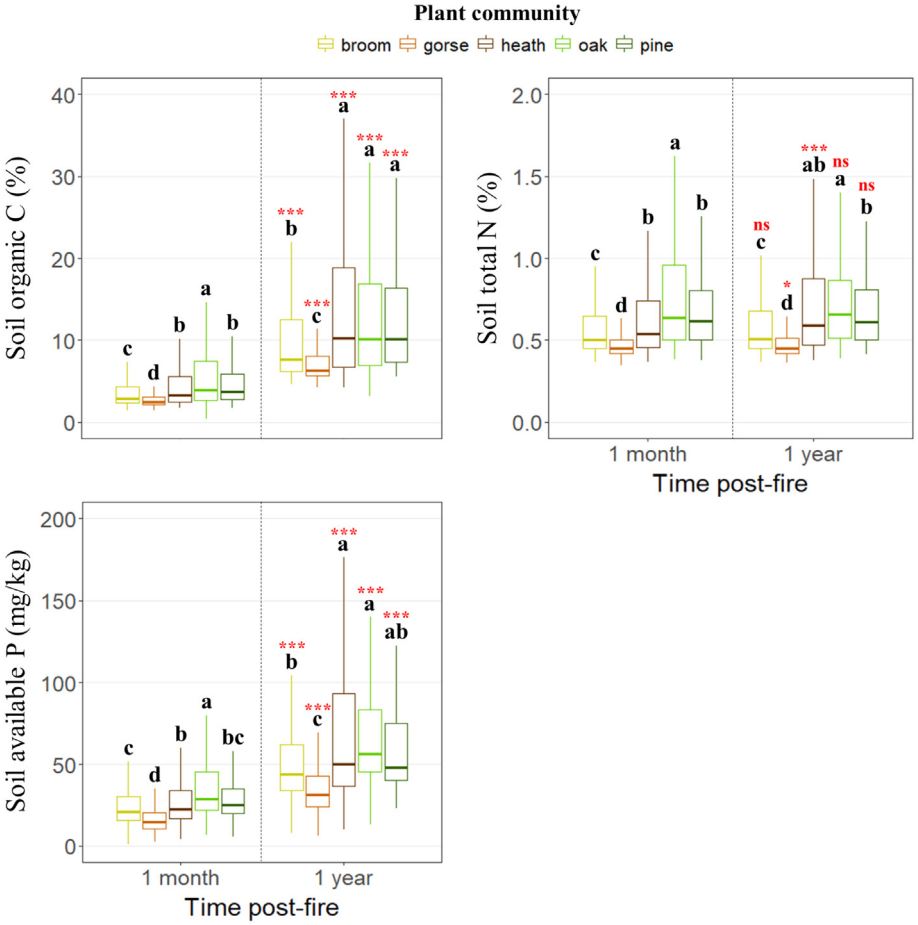

Fig. 6. Boxplots showing the relationship between soil organic C, total N and available P, and plant community type, one month and one year after fire. Lowercase letters denote significant differences in the values of soil properties at the 0.05 level within the time period. The significance of the change in the soil properties relative to the immediate post-fire situation is represented by ***(p-value < 0.001), **(p-value < 0.01), *(p-value < 0.05) and *ns* (p-value > 0.05).

Menéndez-Duarte et al., 2008; Tanase et al., 2015), particularly in areas of complex topography (Tanase et al., 2010). In addition, litter accumulation in the first post-fire periods can significantly affect forest floor emission at L-band (Della-Vecchia et al., 2007; Kalogirou et al., 2014).

4.2. Temporal extrapolation of L-band SAR predictive relationships

The extrapolation of ALOS-2 predictive relationships of soil properties from an immediate post-fire scenario to one year after wildfire exhibited similar performance to that of the internal model validation. In this sense, the existence of non-stationary responses between the reference and target systems in the transferability approach (Osborne et al., 2007), evidenced by the distinct change patterns for each soil property between both temporal scenarios depending on plant community type, did not undermine the attainment of a transferable model. This could be explained by the (i) robust handling of uncertainty in the FMA modeling approach (Nakagawa and Freckleton, 2011), contributing to reduce the bias in model calibration (Tsalyuk et al., 2017) and improving predictive performance in the target system (Dormann et al., 2018), and (ii) the physical sense of SAR backscatter signal in burned landscapes (Kalogirou et al., 2014). Future efforts are needed to verify the transferability of SAR data for monitoring the variability of soil properties in post-fire scenarios with stronger vegetation responses, where increasing volume and dihedral scattering from regenerating forest canopies can be expected (Kasischke et al., 2007; Tanase et al., 2015). In addition, interannual soil moisture variations as a consequence of post-fire weather must be considered in SAR time-series acquisitions (Minchella et al., 2009). Precipitation can temporarily enhance the SAR backscatter coefficient (Belenguer-Plomer et al., 2019), the increase being dependent on the vegetation cover as a function of vegetation succession in different plant communities (Kasischke et al., 2007), reducing SAR backscatter sensitivity to changes in soil properties.

4.3. Effects of pre-fire plant community on short-term changes of soil properties

The magnitude of change in soil properties, quantified from ALOS-2 based predictions one month and one year after wildfire, was markedly influenced by the pre-fire plant community type. Remarkably, our results for the considered soil properties are consistent with those achieved in previous research based exclusively on small-scale field surveys (e.g. Heath et al., 2015; Fernández-García et al., 2019; Huerta et al., 2020), which proves the potential of SAR backscatter data in the L-band for assessing fire effects on soil properties at large spatial scales. The observed short-term increase in soil organic C content in all plant communities could be related to soil inputs of (i) partially scorched material or litter from decaying vegetation legacies (Murphy et al., 2006; Knicker, 2007; Caon et al., 2014), (ii) unburned legacies from dead roots that slowly incorporate into the soil (Fernández et al., 1999; Brye, 2006) and (iii) litter from fast-recovering resprouter species in the firsts post-fire stages (Knicker et al., 2005). On the other hand, ash deposits and mineralization of organic P from litter and vegetation to orthophosphate, directly available for plant uptake (Noack et al., 2012), may explain the short-term increase observed in available P in each plant community. Conversely, the change in soil total N exhibited a much less clear pattern, featuring a significant increase one year after wildfire in heathlands, but a decrease in gorse shrublands. In this sense, the fire impact on the soil total N pool remains unclear (Alcañiz et al., 2016), with several studies in Mediterranean ecosystems showing

contradictory results even under the same plant communities (Caon et al., 2014; Alcañiz et al., 2018; and references therein).

Huerta et al. (2020) also found through a field-based work that Pyrenean oak forests in the same study site featured the highest soil organic C and nutrients content, being the most fire-resistant community. However, one year after wildfire, we novelty evidenced that soil properties in heathlands and Scots pine forests reached similar values to Pyrenean oak forests. This pattern may be explained by the increase in litterfall and root litter decomposition linked to the high post-fire recovery rates of the dominant resprouter species in heathlands (Valdecantos et al., 2009; Fernández-Guisuraga et al., 2021b) and in the understory of Scots pine forests with greater light availability after wildfire (Vacchiano et al., 2014; Dzwonko et al., 2015).

It should be emphasized that the evidenced post-fire trends in soil organic C and nutrients may reflect a short-term pulse that may not persist for long after fire, as it has been reported worldwide (e.g. Ficken and Wright, 2017; Alexander et al., 2018). However, the observed trends at short-term could be a meaningful driver of post-fire vegetation recovery responses in the first post-fire stages (Dzwonko et al., 2015).

5. Conclusions

Monitoring fire impact on soil through remote sensing techniques in large and heterogeneous burned landscapes is essential to determine the implementation of post-fire emergency actions aimed at mitigating soil degradation. This study is pioneer in evaluating the potential of C-band and L-band SAR data for this purpose. The estimation of soil organic C and nutrients content immediately after fire from L-band SAR backscatter outperforms the retrieval from C-band data because of the lower attenuation of backscatter signal in the L-band by vegetation canopies and increased interaction with soil surface properties. In addition, predictive relationships between soil properties and L-band data can be transferable across post-fire scenarios, supporting the applicability of this approach for monitoring the temporal variability of fire effects on soil properties at reduced cost. Finally, we demonstrate that changes in soil properties at short-term after fire are markedly influenced by pre-fire plant community type.

CRediT authorship contribution statement

José Manuel Fernández-Guisuraga: Conceptualization, Methodology, Formal analysis, Investigation, Writing – original draft. **Elena Marcos:** Conceptualization, Writing – review & editing, Supervision. **Susana Suárez-Seoane:** Conceptualization, Writing – review & editing, Supervision, Project administration, Funding acquisition. **Leonor Calvo:** Conceptualization, Writing – review & editing, Supervision, Project administration, Funding acquisition.

Declaration of competing interest

The authors declare that they have no known competing financial interests or personal relationships that could have appeared to influence the work reported in this paper.

Acknowledgements

This study was financially supported by the Spanish Ministry of Economy and Competitiveness, and the European Regional Development Fund (ERDF), in the framework of the FIRESEVES (AGL2017-86075-C2-1-R) project; and by the Regional Government of Castilla y León in the framework of the WUIFIRECYL (LE005P20) project.

Appendix A. Supplementary data

Supplementary data to this article can be found online at https://doi.org/10.1016/j.scitotenv.2022.156852.

References

AEMET, 2022. AEMET Open Data. Agencia Estatal de Meteorología. http://www.aemet.es/es/datos_abiertos/AEMET_OpenData. (Accessed 2 March 2022).
Alcañiz, M., Outeiro, L., Francos, M., Farguell, J., Úbeda, X., 2016. Long-term dynamics of soil chemical properties after a prescribed fire in a Mediterranean forest (Montgrí massif, Catalonia, Spain). Sci. Total Environ. 572, 1329–1335.
Alcañiz, M., Outeiro, L., Francos, M., Úbeda, X., 2018. Effects of prescribed fires on soil properties: a review. Sci. Total Environ. 613, 944–957.
Aldana-Jague, E., Heckrath, G., Macdonald, A., van Wesemael, B., Van Oost, K., 2016. UAS-based soil carbon mapping using VIS-NIR (480–1000 nm) multi-spectral imaging: potential and limitations. Geoderma 275, 55–66.
Alexander, H.D., Natali, S.M., Loranty, M.M., Ludwig, S.M., Spektor, V.V., Davydov, S., Zimov, N., Trujillo, I., Mack, M.C., 2018. Impacts of increased soil burn severity on larch forest regeneration on permafrost soils of far northeastern Siberia. For. Ecol. Manag. 417, 144–153.
Angelopoulou, T., Tziolas, N., Balafoutis, A., Zalidis, G., Bochtis, D., 2019. Remote sensing techniques for soil organic carbon estimation: a review. Remote Sens. 11, 676.
Barton, K., 2020. MuMIn: Multi-Model Inference. R Package Version 1.43.17. https://CRAN.R-project.org/package=MuMIn.
Bartsch, A., Widhalm, B., Kuhry, P., Hugelius, G., Palmtag, J., Siewert, M.B., 2016. Can C-band synthetic aperture radar be used to estimate soil organic carbon storage in tundra? Biogeosciences 13, 5453–5470.
Belenguer-Plomer, M.A., Tanase, M.A., Fernandez-Carrillo, A., Chuvieco, E., 2019. Burned area detection and mapping using Sentinel-1 backscatter coefficient and thermal anomalies. Remote Sens. Environ. 233, 111345.
Bivand, R., Keitt, T., Rowlingson, B., 2021. rgdal: Bindings for the 'Geospatial' Data Abstraction Library R Package Version 15-23. https://CRANR-projectorg/package=rgdal.
Bourgeau-Chavez, L.L., Kasischke, E.S., Riordan, K., Brunzell, S., Nolan, M., Hyer, Slawski, E.J., Medvecz, M., Walters, T., Ames, S., 2007. Remote monitoring of spatial and temporal surface soil moisture in fire disturbed boreal forest ecosystems with ERS SAR imagery. International Journal of Remote Sensing 28, 2133–2162.
Bousbih, S., Zribi, M., Pelletier, C., Gorrab, A., Lili-Chabaane, Z., Baghdadi, N., Ben Aissa, N., Mougenot, B., 2019. Soil texture estimation using radar and optical data from Sentinel-1 and Sentinel-2. Remote Sens. 11, 1520.
Bouvet, A., Mermoz, S., Le Toan, T., Villard, L., Mathieu, R., Naidoo, L., Asner, G.P., 2018. An above-ground biomass map of African savannahs and woodlands at 25m resolution derived from ALOS PALSAR. Remote Sens. Environ. 206, 156–173.
Bremner, J.M., Mulvaney, C.S., 1982. Nitrogen total. In: Page, A.L., Miller, R.H., Keeney, D.R. (Eds.), Methods of Soil Analysis. Part 2: Chemical and Microbiological Properties, second ed. ASA, Madison, United States, pp. 595–624.
Brye, K.R., 2006. Soil physiochemical changes following 12 years of annual burning in a humid–subtropical tallgrass prairie: a hypothesis. Acta Oecol. 30, 407–413.
Burgin, M., Clewley, D., Lucas, R.M., Moghaddam, M., 2011. A generalized radar backscattering model based on wave theory for multilayer multispecies vegetation. IEEE Trans. Geosci. Remote Sens. 49, 4832–4845.
Burnham, K.P., Anderson, D.R., 2002. Model Selection and Multimodel Inference: A Practical Information-Theoretic Approach. Springer, Berlin, Germany.
Caon, L., Ramón Vallejo, V., Ritsema, C.J., Geissen, V., 2014. Effects of wildfire on soil nutrients in Mediterranean ecosystems. Earth Sci. Rev. 139, 47–58.
Ceddia, M.B., Gomes, A.S., Vasques, G.M., Pinheiro, É.F.M., 2017. Soil carbon stock and particle size fractions in the central amazon predicted from remotely sensed relief, multispectral and radar data. Remote Sensing 9, 124.
Della-Vecchia, A., Ferrazzoli, P., Wigneron, J., Grant, J.P., 2007. Modeling Forest emissivity at L-band and a comparison with multitemporal measurements. IEEE Geosci. Remote Sens. Lett. 4, 508–512.
Dormann, C.F., Calabrese, J.M., Guillera-Arroita, G., Matechou, E., Bahn, V., Bartoń, K., Beale, C.M., Ciuti, S., Elith, J., Gerstner, K., Guelat, J., Keil, P., Lahoz-Monfort, J.J., Pollock, L.J., Reineking, B., Roberts, D.R., Schröder, B., Thuiller, W., Warton, D.I., Wintle, B.A., Wood, S.N., Wüest, R.O., Hartig, F., 2018. Model averaging in ecology: a review of Bayesian, information-theoretic, and tactical approaches for predictive inference. Ecol. Monogr. 88, 485–504.
Dumas, J.B.A., 1831. Procedes de l'analyse organic. Ann. Chim. Phys. 247, 198–213.
Dzwonko, Z., Loster, S., Gawroński, S., 2015. Impact of fire severity on soil properties and the development of tree and shrub species in a scots pine moist forest site in southern Poland. For. Ecol. Manag. 342, 56–63.
El Hajj, M., Baghdadi, N., Bazzi, H., Zribi, M., 2019. Penetration analysis of SAR signals in the C and L bands for wheat, maize, and grasslands. Remote Sens. 11, 31.
ESA, 2022. Sentinel-1 SAR User Guide. https://sentinels.copernicus.eu/web/sentinel/user-guides/sentinel-1-sar. (Accessed 2 March 2022).
ESA, 2022. Sentinel-1 Mission. https://sentinel.esa.int/web/sentinel/missions/sentinel-1. (Accessed 2 March 2022).
ESA, 2022. Sentinel Application Platform (SNAP). https://earth.esa.int/eogateway/tools/snap. (Accessed 2 March 2022).
European Commission, 2021. EU Soil Strategy for 2030. COM(2021) 699 Final.
Fernández, I., Cabaneiro, A., Carballas, T., 1999. Carbon mineralization dynamics in soils after wildfires in two Galician forests. Soil Biol. Biochem. 31, 1853–1865.
Fernández-García, V., Miesel, J., Baeza, M.J., Marcos, E., Calvo, L., 2019. Wildfire effects on soil properties in fire-prone pine ecosystems: indicators of burn severity legacy over the medium term after fire. Appl. Soil Ecol. 135, 147–156.
Fernández-Guisuraga, J.M., Suárez-Seoane, S., Calvo, L., 2019a. Modeling Pinus pinaster forest structure after a large wildfire using remote sensing data at high spatial resolution. For. Ecol. Manag. 446, 257–271.
Fernández-Guisuraga, J.M., Calvo, L., Fernández-García, V., Marcos-Porras, E., Taboada, A., Suárez-Seoane, S., 2019b. Efficiency of remote sensing tools for post-fire management along a climatic gradient. For. Ecol. Manag. 433, 553–562.

Fernández-Guisuraga, J.M., Suárez-Seoane, S., García-Llamas, P., Calvo, L., 2021a. Vegetation structure parameters determine high burn severity likelihood in different ecosystem types: a case study in a burned Mediterranean landscape. J. Environ. Manag. 288, 112462.

Fernández-Guisuraga, J.M., Suárez-Seoane, S., Calvo, L., 2021b. Radiative transfer modeling to measure fire impact and forest engineering resilience at short-term. ISPRS J. Photogramm. Remote Sens. 176, 30–41.

Fernandez-Martinez, M., Vicca, S., Janssens, I.A., Sardans, J., Luyssaert, S., Campioli, M., Chapin, F.S., Ciais, P., Malhi, Y., Obersteiner, M., Papale, D., Piao, S.L., Reichstein, M., Roda, F., Penuelas, J., 2014. Nutrient availability as the key regulator of global forest carbon balance. Nat. Clim. Chang. 4, 471–476.

Ficken, C.D., Wright, J.P., 2017. Contributions of microbial activity and ash deposition to post-fire nitrogen availability in a pine savanna. Biogeosciences 14, 241–255.

Freckleton, R.P., 2010. Dealing with collinearity in behavioral and ecological data: model averaging and the problems of measurement error. Behav. Ecol. Sociobiol. 65, 91–101.

GEODE, 2022. Mapa Geológico Digital continuo de España. http://mapas.igme.es/gis/services/Cartografia_Geologica/IGME_Geode_50/MapServer/WMSServer/. (Accessed 31 January 2022).

Gholizadeh, A., Žižala, D., Saberioon, M., Borůvka, L., 2018. Soil organic carbon and texture retrieving and mapping using proximal, airborne and Sentinel-2 spectral imaging. Remote Sens. Environ. 218, 89–103.

Grueber, C.E., Nakagawa, S., Laws, R.J., Jamieson, I.G., 2011. Multimodel inference in ecology and evolution: challenges and solutions. J. Evol. Biol. 24, 699–711.

Heath, J.T., Chafer, C.J., Bishop, T.F.A., Van Ogtrop, F.F., 2015. Wildfire effects on soil carbon and water repellency under eucalyptus forest in eastern Australia. Soil Res. 53, 13–23.

Hijmans, R.J., 2021. raster: Geographic Data Analysis and Modeling R Package Version 34-10. https://CRANR-projectorg/package=raster.

Holdo, R.M., Mack, M.C., Arnold, S.G., 2012. Tree canopies explain fire effects on soil nitrogen, phosphorus and carbon in a savanna ecosystem. J. Veg. Sci. 23, 352–360.

Hudak, A.T., Morgan, P., Bobbitt, M.J., Smith, A.M.S., Lewis, S.A., Lentile, L.B., Robichaud, P.R., Clark, J.T., McKinley, R.A., 2007. The relationship of multispectral satellite imagery to immediate fire effects. Fire Ecol. 3, 64–90.

Huerta, S., Fernández-García, V., Calvo, L., Marcos, E., 2020. Soil resistance to burn severity in different Forest ecosystems in the framework of a wildfire. Forests 11, 773.

Hurvich, C.M., Tsai, C.-L., 1989. Regression and time series model selection in small samples. Biometrika 76, 297–307.

Inoue, A., Kurosu, T., Maeno, H., Uratsuka, S., Kozu, T., Dabrowska-Zielinska, K., Qi, J., 2002. Season-long daily measurements of multifrequency (Ka, Ku, X, C, and L) and full-polarization backscatter signatures over paddy rice field and their relationship with biological variables. Remote Sensing of Environment 81, 194–204.

ITACyL, 2022. Proyecto SUELOS. http://ftp.itacyl.es/Edafologia/. (Accessed 31 January 2022).

Jagdhuber, T., 2012. Soil Parameter Retrieval Under Vegetation Cover Using SAR Polarimetry. University of Potsdam, Germany Thesis Dissertation.

JAXA, 2022. ALOS-2 Project/PALSAR-2. https://www.eorc.jaxa.jp/ALOS-2/en/about/palsar2.htm. (Accessed 2 March 2022).

Johnson, D.W., Turner, J., 2019. Tamm review: nutrient cycling in forests: a historical look and newer developments. For. Ecol. Manag. 444, 344–373.

Johnstone, J.F., Chapin, F.S., 2006. Effects of soil burn severity on post-fire tree recruitment in boreal forest. Ecosystems 9, 14–31.

Kalogirou, V., Ferrazzoli, P., Vecchia, A.D., Foumelis, M., 2014. On the SAR backscatter of burned forests: a model-based study in C-band, over burned pine canopies. IEEE Trans. Geosci. Remote Sens. 52, 6205–6215.

Kasischke, E.S., Bourgeau-Chavez, L.L., Johnstone, J.F., 2007. Assessing spatial and temporal variations in surface soil moisture in fire-disturbed black spruce forests in interior Alaska using spaceborne synthetic aperture radar imagery — implications for post-fire tree recruitment. Remote Sens. Environ. 108, 42–58.

Kassambara, A., 2021. rstatix: Pipe-friendly Framework for Basic Statistical Tests. R Package Version 0.7.0. https://CRAN.R-project.org/package=rstatix.

Knicker, H., 2007. How does fire affect the nature and stability of soil organic nitrogen and carbon? A review. Biogeochemistry 85, 91–118.

Knicker, H., González-Vila, F.J., Polvillo, O., González, J.A., Almendros, G., 2005. Fire-induced transformation of C- and N-forms in different organic soil fractions from a dystric cambisol under a Mediterranean pine forest (Pinus pinaster). Soil Biol. Biochem. 37, 701–718.

Kovács, Z.A., Mészáros, J., Árvai, M., Laborczi, A., Szatmári, G., László, P., Pásztor, L., 2021. Testing PRISMA hyperspectral satellite imagery in predicting soil carbon content based on synthetized LUCAS spectral data. EGU General Assembly 2021, EGU21-15450.

Kuhn, M., 2020. caret: Classification and Regression Training R Package Version 60-86. https://CRANR-projectorg/package=caret.

Le, N.N., Pham, T.D., Yokoya, N., Ha, N.T., Nguyen, T.T.T., Tran, T.D.T., Pham, T.D., 2021. Learning from multimodal and multisensor earth observation dataset for improving estimates of mangrove soil organic carbon in Vietnam. Int. J. Remote Sens. 42, 6866–6890.

Liang, C., Amelung, W., Lehmann, J., Kästner, M., 2019. Quantitative assessment of microbial necromass contribution to soil organic matter. Glob. Chang. Biol. 25, 3578–3590.

Liu, E., Yan, C., Mei, X., He, W., Bing, S.H., Ding, L., Liu, Q., Liu, S., Fan, T., 2010. Long-term effect of chemical fertilizer, straw, and manure on soil chemical and biological properties in Northwest China. Geoderma 158, 173–180.

Liu, C., Shang, J., Vachon, P.W., McNairn, H., 2013. Multiyear crop monitoring using polarimetric RADARSAT-2 data. IEEE Trans. Geosci. Remote Sens. 51, 2227–2240.

Lucas-Borja, M.E., Delgado-Baquerizo, M., Muñoz-Rojas, M., Plaza-Álvarez, P.A., Gómez-Sanchez, M.E., González-Romero, J., Peña-Molina, E., Moya, D., de las Heras, J., 2021. Changes in ecosystem properties after post-fire management strategies in wildfire-affected Mediterranean forests. Journal of Applied Ecology 58, 836–846.

Luo, Z., Feng, W., Luo, Y., Baldock, J., Wang, E., 2017. Soil organic carbon dynamics jointly controlled by climate, carbon inputs, soil properties and soil carbon fractions. Glob. Chang. Biol. 23, 4430–4439.

Maestre, F.T., Quero, J.L., Gotelli, N.J., Escudero, A., Ochoa, V., Delgado-Baquerizo, M., García-Gómez, M., Bowker, M.A., Soliveres, S., Escolar, C., García-Palacios, P., Berdugo, M., Valencia, E., Gozalo, B., Gallardo, A., Aguilera, L., Arredondo, T., Blones, J., Boeken, B., Bran, D., Conceição, A.A., Cabrera, O., Chaieb, M., Derak, M., Eldridge, D.J., Espinosa, C.I., Florentino, A., Gaitán, J., Gatica, M.G., Ghiloufi, W., Gómez-González, S., Gutiérrez, J.R., Hernández, R.M., Huang, X., Huber-Sannwald, E., Jankju, M., Miriti, M., Monerris, J., Mau, R.L., Morici, E., Naseri, K., Ospina, A., Polo, V., Prina, A., Pucheta, E., Ramírez-Collantes, D.A., Romão, R., Tighe, M., Torres-Díaz, C., Val, J., Veiga, J.P., Wang, D., Zaady, E., 2012. Plant species richness and ecosystem multifunctionality in global drylands. Science 335 (6065), 214–218.

Maynard, J.J., Levi, M.R., 2017. Hyper-temporal remote sensing for digital soil mapping: characterizing soil-vegetation response to climatic variability. Geoderma 285, 94–109.

Menéndez-Duarte, R., Wozniak, E., Recondo, C., Cabo, C., Marquínez, J., Fernández, S., 2008. Estimation of surface roughness and stone cover in burnt soils using SAR images. Catena 74, 264–272.

Mermoz, S., Réjou-Méchain, M., Villard, L., Le Toan, T., Rossi, V., Gourlet-Fleury, S., 2015. Decrease of L-band SAR backscatter with biomass of dense forests. Remote Sens. Environ. 159, 307–317.

Minchella, A., Del Frate, F., Capogna, F., Anselmi, S., Manes, F., 2009. Use of multitemporal SAR data for monitoring vegetation recovery of Mediterranean burned areas. Remote Sens. Environ. 113, 588–597.

Minu, S., Shetty, A., Minasny, B., Gomez, C., 2017. The role of atmospheric correction algorithms in the prediction of soil organic carbon from hyperion data. Int. J. Remote Sens. 38, 6435–6456.

Mirzaee, S., Ghorbani-Dashtaki, S., Mohammadi, J., Asadi, H., Asadzadeh, F., 2016. Spatial variability of soil organic matter using remote sensing data. Catena 145, 118–127.

Mitchard, E.T.A., Saatchi, S.S., White, L.J.T., Abernethy, K.A., Jeffery, K.J., Lewis, S.L., Collins, M., Lefsky, M.A., Leal, M.E., Woodhouse, I.H., Meir, P., 2012. Mapping tropical forest biomass with radar and spaceborne LiDAR in Lopé National Park, Gabon: overcoming problems of high biomass and persistent cloud. Biogeosciences 9, 179–191.

Moreno, J.M., Oechel, W.C., 1994. The Role of Fire in Mediterranean-type Ecosystems. Springer, New York, United States.

Morgan, P., Keane, P.E., Dillon, G.K., Jain, T.B., Hudak, A.T., Karau, E.C., Sikkink, P.G., Holden, A.A., Strand, E.K., 2014. Challenges of assessing fire and burn severity using field measures, remote sensing and modelling. Int. J. Wildland Fire 23, 1045–1060.

Moser, K.F., Ahn, C., Noe, G.B., 2009. The influence of microtopography on soil nutrients in created mitigation wetlands. Restor. Ecol. 17, 641–651.

Murphy, J.D., Johnson, D.W., Miller, W.W., Walker, R.F., Carroll, E.F., Blank, R.R., 2006. Wildfire effects on soil nutrients and leaching in a Tahoe Basin watershed. J. Environ. Qual. 35, 479–489.

Mzid, N., Castaldi, F., Tolomio, M., Pascucci, S., Casa, R., Pignatti, S., 2022. Evaluation of agricultural bare soil properties retrieval from landsat 8, Sentinel-2 and PRISMA satellite data. Remote Sens. 14, 714.

Nakagawa, S., Freckleton, R.P., 2011. Model averaging, missing data and multiple imputation: a case study for behavioural ecology. Behav. Ecol. Sociobiol. 65, 103–116.

Nguyen, T.T., Pham, T.D., Nguyen, C.T., Delfos, J., Archibald, R., Dang, K.B., Hoang, N.B., Guo, W., Ngo, H.H., 2022. A novel intelligence approach based active and ensemble learning for agricultural soil organic carbon prediction using multispectral and SAR data fusion. Sci. Total Environ. 804, 150187.

Ninyerola, M., Pons, X., Roure, J.M., 2005]. Atlas Climático Digital de la Península Ibérica. Metodología y aplicaciones en bioclimatología y geobotánica. [dataset]Universidad Autónoma de Barcelona.

Noack, S.R., McLaughlin, M.J., Smernik, R.J., McBeath, T.M., Armstrong, R.D., 2012. Crop residue phosphorus: speciation and potential bio-availability. Plant Soil 359, 375–385.

Olsen, S.R., Cole, C.V., Frank, S.W., Dean, L.A., 1954. Estimation of available phosphorus in soils by extraction with sodium bicarbonate. USDA Circular No. 939. US Government Printing Office, Washington DC, USA, p. 19.

Osborne, P.E., Foody, G.M., Suárez-Seoane, S., 2007. Non-stationarity and local approaches to modelling the distributions of wildlife. Divers. Distrib. 13, 313–323.

Pausas, J., Keely, J.E., 2009. A burning story: the role of fire in the history of life. Bioscience 59, 593–601.

Philipp, M.B., Levick, S.R., 2020. Exploring the potential of C-band SAR in contributing to burn severity mapping in tropical savanna. Remote Sens. 12, 49.

Picotte, J.J., Robertson, K.M., 2011. Validation of remote sensing of burn severity in south-eastern US ecosystems. Int. J. Wildland Fire 20, 453–464.

Pulliainen, J.T., Mikhela, P.J., Hallikainen, M.T., Ikonen, J.-P., 1996. Seasonal dynamics of C-band backscatter of boreal forests with applications to biomass and soil moisture estimation. IEEE Trans. Geosci. Remote Sens. 34, 758–770.

R Core Team, 2021. R: A language and environment for statistical computing. R Foundation for Statistical Computing, Vienna, Austria https://www.R-project.org/.

Rossel, R.A.V., Bui, E.N., 2016. A new detailed map of total phosphorus stocks in Australian soil. Sci. Total Environ. 542, 1040–1049.

Santoro, M., Cartus, O., Fransson, J.E.S., 2022. Dynamics of the swedish forest carbon pool between 2010 and 2015 estimated from satellite L-band SAR observations. Remote Sens. Environ. 270, 112846.

Schönbrodt-Stitt, S., Ahmadian, N., Kurtenbach, M., Conrad, C., Romano, N., Bogena, H.R., Vereecken, H., Nasta, P., 2021. Statistical exploration of SENTINEL-1 data, terrain parameters, and in-situ data for estimating the near-surface soil moisture in a Mediterranean agroecosystem. Front. Water 3, 655837.

Shimada, M., Ohtaki, T., 2010. Generating large-scale high-quality SAR mosaic datasets: application to palsar data for global monitoring. IEEE Trans. Geosci. Remote Sens. 3, 637–656.

Small, D., 2011. Flattening gamma: radiometric terrain correction for SAR imagery. IEEE Trans. Geosci. Remote Sens. 49, 3081–3093.

Small, D., Schubert, A., 2008. Guide to ASAR Geocoding, RSL-ASAR-GC-AD, Issue 1.0.

Stockmann, U., Adams, M.A., Crawford, J.W., Field, D.J., Henakaarchchi, N., Jenkins, M., Minasny, B., McBratney, A.B., Courcelles, V.R., Singh, K., Wheeler, I., Abbott, L., Angers, D.A., Baldock, J., Bird, M., Brookes, P.C., Chenu, C., Jastrow, J.D., Lal, R., Lehmann, J., O'Donnell, A.G., Parton, W.J., Whitehead, D., Zimmermann, M., 2013. The knowns, known unknowns and unknowns of sequestration of soil organic carbon. Agric. Ecosyst. Environ. 164, 80–99.

Strahler, A.H., 1980. The use of prior probabilities in maximum likelihood classification of remotely sensed data. Remote Sens. Environ. 10, 135–163.

Tanase, M.A., Santoro, M., de la Riva, J., Pérez-Cabello, F., Le Toan, T., 2010. Sensitivity of X-, C-, and L-band SAR backscatter to burn severity in Mediterranean pine forests. IEEE Trans. Geosci. Remote Sens. 48, 3663–3675.

Tanase, M.A., Santoro, M., Aponte, C., de la Riva, J., 2014. Polarimetric properties of burned forest areas at C- and L-band. IEEE J. Sel. Top. Appl. Earth Obs. Remote Sens. 7, 267–276.

Tanase, M.A., Kennedy, R., Aponte, C., 2015. Radar burn ratio for fire severity estimation at canopy level: an example for temperate forests. Remote Sens. Environ. 170, 14–31.

Tanase, M.A., Belenguer-Plomer, M.A., Roteta, E., Bastarrika, A., Wheeler, J., Fernández-Carrillo, Á., Tansey, K., Wiedemann, W., Navratil, P., Lohberger, S., Siegert, F., Chuvieco, E., 2020. Burned area detection and mapping: intercomparison of Sentinel-1 and Sentinel-2 based algorithms over tropical Africa. Remote Sens. 12, 334.

Tsalyuk, M., Kelly, M., Getz, W.M., 2017. Improving the prediction of african savanna vegetation variables using time series of MODIS products. ISPRS J. Photogramm. Remote Sens. 131, 77–91.

Vacchiano, G., Stanchi, S., Marinari, G., Ascoli, D., Zanini, E., Motta, R., 2014. Fire severity, residuals and soil legacies affect regeneration of scots pine in the southern Alps. Sci. Total Environ. 472, 778–788.

Valdecantos, A., Baeza, M.J., Vallejo, V.R., 2009. Vegetation management for promoting ecosystem resilience in fire-prone Mediterranean shrublands. Restor. Ecol. 17, 414–421.

Vieira, D.C.S., Fernández, C., Vega, J.A., Keizer, J.J., 2015. Does soil burn severity affect the post-fire runoff and interrill erosion response? A review based on meta-analysis of field rainfall simulation data. J. Hydrol. 523, 452–464.

Wang, Y.P., Law, R.M., Pak, B., 2010. A global model of carbon, nitrogen and phosphorus cycles for the terrestrial biosphere. Biogeosciences 7, 2261–2282.

Wang, X., Zhang, Y., Atkinson, P.M., Yao, H., 2020. Predicting soil organic carbon content in Spain by combining landsat TM and ALOS PALSAR images. Int. J. Appl. Earth Obs. Geoinf. 92, 102182.

Whittingham, M.J., Stephens, P.A., Bradbury, R.B., Freckleton, R.P., 2006. Why do we still use stepwise modelling in ecology and behaviour? J. Anim. Ecol. 75, 1182–1189.

Williams, M.L., Mitchell, A.L., Milne, A.K., Danaher, T., Horn, G., 2022. Addressing critical influences on L-band radar backscatter for improved estimates of basal area and change. Remote Sens. Environ. 272, 112933.

Yang, R.M., Guo, W.W., 2019. Using time-series Sentinel-1 data for soil prediction on invaded coastal wetlands. Environ. Monit. Assess. 191, 462.

Yang, R.-M., Guo, W.-W., Zheng, J.-B., 2019. Soil prediction for coastal wetlands following Spartina alterniflora invasion using Sentinel-1 imagery and structural equation modeling. Catena 173, 465–470.

Zhang, Y., Ling, F., Foody, G.M., Ge, Y., Boyd, D.S., Li, X., Du, Y., Atkinson, P.M., 2019. Mapping annual forest cover by fusing PALSAR/PALSAR-2 and MODIS NDVI during 2007–2016. Remote Sens. Environ. 224, 74–91.

Zhou, T., Geng, Y., Chen, J., Pan, J., Haase, D., Lausch, A., 2020. High-resolution digital mapping of soil organic carbon and soil total nitrogen using DEM derivatives, Sentinel-1 and Sentinel-2 data based on machine learning algorithms. Sci. Total Environ. 729, 138244.

Zhou, T., Geng, Y., Ji, C., Xu, X., Wang, H., Pan, J., Bumberger, J., Haase, D., Lausch, A., 2021. Prediction of soil organic carbon and the C: N ratio on a national scale using machine learning and satellite data: a comparison between Sentinel-2, Sentinel-3 and Landsat-8 images. Sci. Total Environ. 755, 142661.

Zribi, M., Dechambre, M., 2003. A new empirical model to retrieve soil moisture and roughness from C-band radar data. Remote Sens. Environ. 84, 42–52.

Zuur, A.F., Ieno, E.N., Walker, N., Saveliev, A.A., Smith, G.M., 2009. Mixed Effects Models and Extensions in Ecology with R. Springer, New York, United States.